



# Experimental Study on the Failure Modes of Reinforced Loess Slopes with Frame Pre-stressed Anchors under Rainfall Influence

Yanpeng Zhu<sup>a</sup>, Ao Wang<sup>\*</sup>, Anping Huang<sup>b</sup>, Linping Wu<sup>c</sup>, Dong Cheng<sup>d</sup>

Lanzhou University of Technology, Lanzhou, 730050, China

<sup>a</sup>zhuyp1@163.com, <sup>\*</sup>2512411422@qq.com

<sup>b</sup>huanganping1995@163.com, <sup>c</sup>wlping0916@163.com

<sup>d</sup>ddong1996@163.com

**Abstract.** The stability of loess slopes reinforced with frame pre-stressed anchors is often compromised under the influence of rainfall, yet the destabilization modes and triggering factors remain unclear. To address this issue, indoor model experiments were conducted under simulated rainfall conditions, monitoring parameters such as slope moisture content to analyze the failure modes of loess slopes reinforced with frame anchors during rainfall. The results indicate rainwater infiltration increases the volumetric water content and pore water pressure of the slope, decreases the matrix suction, and decreases the migration rate of the wetting front. The axial force of the bolt increases linearly and then decreases, and finally remains stable. The axial distribution pattern of the bolt axial force has not changed fundamentally. A significant correlation between slope instability and the rainfall infiltration process, along with the resulting parameter changes. The post-reinforcement evolution of slope cracks is characterized by small cracks, followed by transverse cracks penetrating the rear edge, and longitudinal shear cracks in the middle of the slope. The failure mode of the reinforced slope shifts from deep-seated landslide before reinforcement to erosion-induced gully formation after reinforcement. This includes shoulder erosion, toe erosion, development of rear-edge cracks, potential sliding surfaces, and gully formation. Preventive measures are proposed to provide references for the design and disaster prevention of slope reinforcement in the northwest region.

**Keywords:** Rainfall Influence; Frame Pre-stressed Anchors; Loess Slope; Failure Modes; Model Experiment.

## 1 Introduction

In recent years, the rapid pace of new infrastructure construction in the northwest region has led to the formation of numerous loess slopes. Loess, characterized by large pores and water sensitivity, is susceptible to the impact of rainfall. To enhance the stability of these slopes, the common engineering practice involves reinforcing them with frame pre-stressed anchor support structures <sup>[1]</sup>. However, with the extended service life of

these support structures and an increase in extreme weather events such as heavy rainfall, some reinforced slopes still experience instability under continuous rainfall conditions. Therefore, studying the stability of loess slopes reinforced with frame prestressed anchors under the influence of rainfall is crucial for disaster prevention and reduction in the northwest region.

For the past few years, many scholars have conducted research on the stability of reinforced slope engineering under rainfall conditions through theoretical derivation, numerical simulation, and indoor and outdoor experiments. Sun et al. [2] conducted real-time studies on the internal seepage field of unsaturated soil slopes under rainfall conditions, obtaining analytical solutions for the slope seepage field and proposing a minimum potential energy stability analysis method. Li et al. [3] improved the infiltration model through finite element software, obtaining a simplified infiltration model for shallow landslides. Kawai, K et al. [4] used the finite element software to simulate slope rainfall infiltration under different slope and rainfall intensity conditions, obtained its hydraulic parameters, and proposed a method for analyzing slope stability based on unsaturated soil mechanics. Di Matteo L et al. [5] conducted experiments with PR2/6 probes that reliably characterized water content and came up with a more reliable theta estimate to evaluate shallow landslides. Guo et al. [6] simulated the stability of reinforced slopes under rainfall conditions using finite element software, analyzing the variation patterns of internal forces in the reinforcement structure and slope stability during rainfall infiltration. In comparison to theoretical derivation and numerical simulation, indoor model experiments are easier to control and observe, providing a more reliable method for studying rainfall-induced slope failure. Zou et al. [7] conducted indoor physical model experiments, analyzing the variation patterns of mechanical parameters before and after rainfall, offering insights for the study of slope reinforcement design. However, current experimental research on rainfall-induced slope failure mainly focuses on the changes in mechanical parameters, with limited studies on the failure modes of reinforced loess slopes. The corresponding instability modes and inducing factors for loess slopes reinforced with frame anchors remain unclear.

Compared with other methods, model experiments can not only visually observe the soil failure situation, accurately obtain the required slope parameters, but also combine theoretical research with engineering practice, thus providing scientific basis for the effective treatment of slope. In this context, this paper selects a typical frame-anchored reinforced loess slope in the northwest region and conducts model experiments. Through monitoring mechanical parameters such as slope moisture content and pore water pressure, the paper analyzes the failure mode of frame-anchored reinforced loess slopes induced by rainfall, proposes preventive measures, and provides references for the stability analysis and reinforcement design of loess slopes under rainfall conditions.

## 2 Experimental Overview

### 2.1 Similarity Ratio Design

The prototype slope is a single-tier loess slope reinforced with frame anchors, with a height of 12 m and a slope of  $80^\circ$ . The retaining board has a thickness of 100 mm, and the cross-sectional dimensions of the frame columns and beams are  $300 \text{ mm} \times 300 \text{ mm}$ . C30 concrete is used for construction, with anchor rod spacing of 3 m and a  $10^\circ$  angle with the horizontal direction. The model box used for the experiment has dimensions of  $3.30 \text{ m} \times 1.60 \text{ m} \times 2.80 \text{ m}$ . Based on the dimensions of the prototype slope and the model box, a geometric similarity ratio  $C_L$  of 10 is applied, as shown in Figure 1.

According to seepage and runoff analysis, the  $We$  criterion [8] is adopted as the rainfall similarity criterion. Basic dimensional quantities for geometric size, density, and gravitational acceleration are used, and based on the second similarity theorem, the relationships and constants for various parameters are obtained, as shown in Table 1.

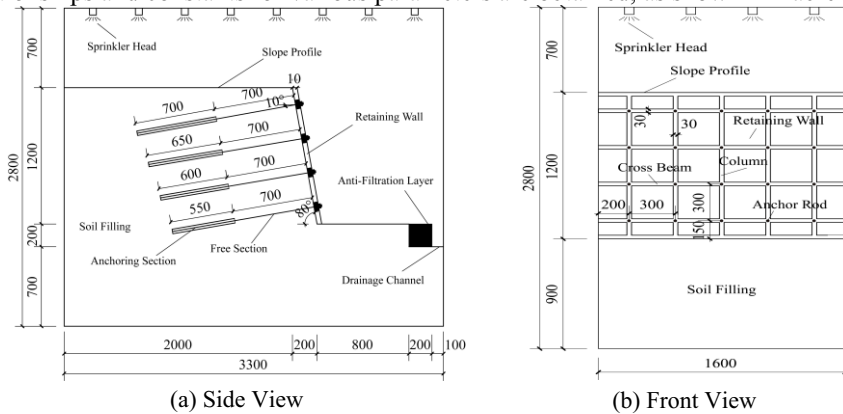


Fig. 1. Schematic Diagram of Model Dimensions /mm

### 2.2 Experimental Materials

The soil samples for the experiment are taken from the prototype slope, and they exhibit uniform characteristics. Classified by particle composition, the soil is identified as loess-like silt. The basic physical and mechanical properties are presented in Table 2. The soil samples are sieved, and water is sprayed to control the moisture content to around 15%. In the subsequent filling process, layer-by-layer construction is employed. The required amount of soil for each layer is calculated based on the compacted dry density, and it is evenly spread and compacted layer by layer in the model box to ensure a compaction degree of 0.85.

In the support structure, the anchor rod body is made of HPB300-grade steel with a diameter of 6 mm. The reinforcing steel in the retaining board is made of galvanized iron wire mesh with a diameter of 1.2 mm. The longitudinal reinforcement in the beams and columns consists of galvanized iron wire with a diameter of 2.8 mm, and the stirrups are made of galvanized iron wire with a diameter of 1.2 mm. The frame and anchor

rod anchoring section are cast using M30-grade cement mortar with a mixing ratio of cement: sand: water = 0.343:1:0.236. The cement strength grade is 42.5, and the sand used is ISO standard sand with particle sizes ranging from 0.08 to 2 mm.

**Table 1.** Similarity Relationships and Constants

Parameter Name	Similarity Relationship	Similarity Constant
Geometric Size	$C_L$	10
Density	$C_\rho$	1
Gravitational Acceleration	$C_g$	1
Stress	$C_\sigma = C_\rho C_g C_L$	10
Strain	$C_\varepsilon = 1$	1
Displacement	$C_s = C_L$	10
Cohesive Force	$C_c = C_\sigma$	10
Internal Friction Angle	$C_\phi = 1$	1
Rainfall Intensity	$C_q = C_L^{-0.5}$	0.32
Rainfall Duration	$C_t = C_L^{1.5}$	31.62
Rainfall Amount	$C_Q = C_L$	10

**Table 2.** Basic Physical and Mechanical Properties

Natural Dry Density /( $\text{g}\cdot\text{cm}^{-3}$ )	Saturated Permeability Co- efficient /(cm $\cdot$ s $^{-1}$ )	Maximum Dry Density /( $\text{g}\cdot\text{cm}^{-3}$ )	Cohesive Force/kPa	Internal Friction Angle/ $^\circ$
1.42	$2.8\times 10^{-5}$	1.66	15	24

### 2.3 Experimental Instruments

To measure the variations in volumetric water content, pore water pressure, and anchor rod axial force, the experimental instruments mainly consist of an artificial rainfall device, moisture sensors, pore water pressure gauges, axial force gauges, strain gauges, DH3816N dynamic data acquisition instrument, and a moisture data acquisition instrument. The arrangement of sensors is illustrated in Figure 2.

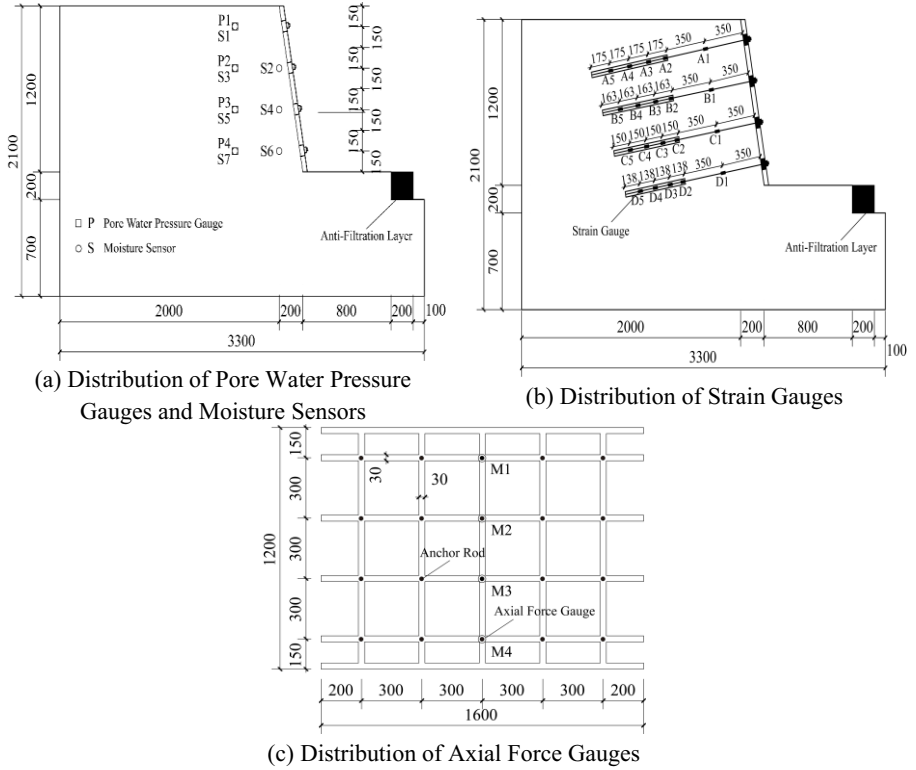


Fig. 2. Sensor Arrangement

Figure 3 shows an artificial rainfall device designed and fabricated according to experimental requirements. To simulate real rainfall conditions, atomizing nozzles are used to reduce the initial velocity of raindrops, minimizing the erosive effect on the slope surface. Before the experiment, the rainfall amount is determined using a rain gauge. The rainfall intensity is calibrated to be approximately 45 mm/h, and the uniformity of rainfall is measured to be 94%, meeting the requirement of over 80%.

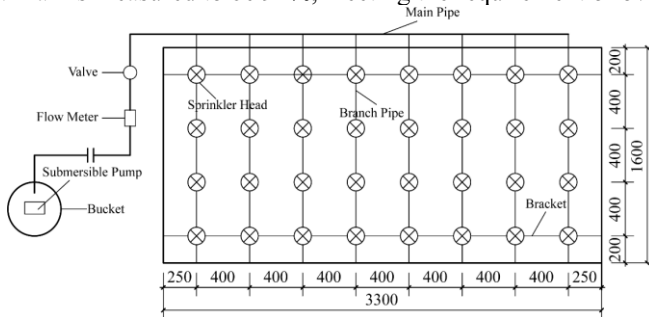


Fig. 3. Design of Artificial Rainfall Devices

## 2.4 Experimental Conditions

The experiment is designed with one set of conditions, featuring rainfall during the period from 8:00 to 21:30 daily. Within this timeframe, a cycle of rainfall at an intensity of 45 mm/h for 30 minutes followed by a 60-minute interval is repeated nine times each day.

## 3 Experimental Results Analysis

### 3.1 Volumetric Water Content Variation

Figure 4 shows the variation of volumetric water content at different measurement points over time. At the start of rainfall, before the wetting front reaches the measurement points, the water content remains at its initial value. As rainwater infiltrates, the wetting front gradually reaches the measurement points, causing a rapid increase in water content. The ponding water at the slope top continues to infiltrate, leading to a continued increase in water content even after rainfall ceases. During the infiltration phase, water content decreases and stabilizes gradually, exhibiting a quasi-periodic variation in the later stages.

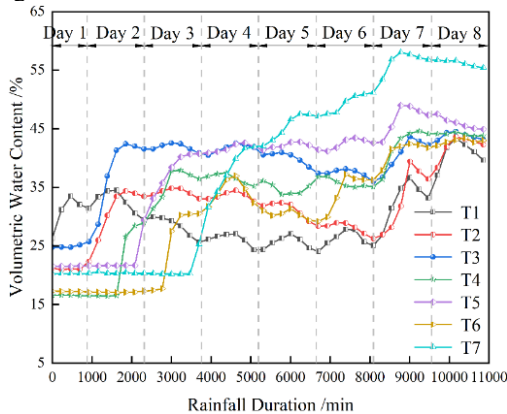


**Fig. 4.** Variation of Volumetric Water Content with Rainfall Duration

(1) The response of volumetric water content to rainfall follows a distinct sequence. The response of deep soil moisture content is observed later than that of shallow soil, and the response of soil moisture in the middle of the slope is observed later than that below the slope surface. This is due to the presence of a gap between the retaining board and the slope model, forming preferential pathways.

(2) Assuming vertical infiltration at the slope top and horizontal infiltration below the slope surface, the migration rate of the wetting front can be approximately estimated using response time and infiltration depth, as shown in Table 3. The data indicates that the average migration rate of the wetting front below the slope surface is approximately  $0.553 \times 10^{-3}$  m/min, while the average migration rate perpendicular to the slope top is  $0.388 \times 10^{-3}$  m/min. As the depth increases, the migration rate of the wetting front

gradually decreases, with the horizontal migration rate slightly greater than the vertical migration rate.

**Table 3.** Migration Rates of the Wetting Front

Location	Below Slope Surface			Middle of Slope		
Sensor Number	S2	S4	S6	S3	S5	S7
Migration Distance/m	0.536	0.894	1.251	0.45	0.75	1.05
Migration Time/min	780	1672	2860	880	2090	3575
Migration Rate / ( $10^{-3} \text{ m} \cdot \text{min}^{-1}$ )	0.687	0.535	0.437	0.511	0.359	0.294

### 3.2 Pore Water Pressure Variation

Figure 5 illustrates the variation of pore water pressure at different depths over time. In the early stages of rainfall, the pore water pressure at each measurement point remains at its initial value. As rainwater infiltrates and the wetting front reaches each measurement point, the pore water pressure rapidly increases in succession. During the infiltration phase, as water gradually percolates downward and the upper soil transitions from saturated to unsaturated, the pore water pressure decreases. In the mid-stage of rainfall, as rainwater continues to infiltrate, the pore water pressure at each measurement point gradually stabilizes. In the later stages of rainfall, as the slope forms a potential sliding surface, the pore water pressure at each measurement point rapidly increases. This is because the internal drainage of the slope is obstructed, resulting in excess pore water pressure.

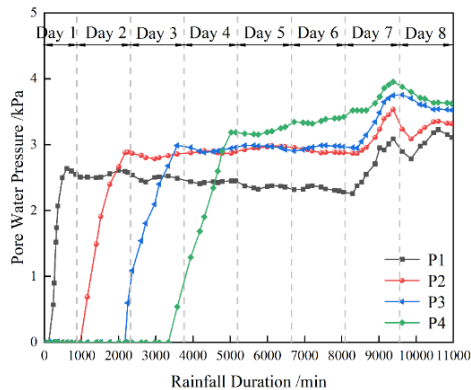


**Fig. 5.** Variation of Pore Water Pressure with Rainfall Duration

It can be observed that the trend of pore water pressure variation is generally consistent with the volumetric water content, but the response of pore water pressure gauges to rainfall infiltration is delayed compared to moisture sensors. This delay is due to the fact that when the wetting front reaches the moisture sensor, the water content changes immediately. However, the wetting front first passes through the permeable stone of the pore water pressure gauge, causing the pore water pressure to change only after the wetting front has passed.

### 3.3 Anchor Rod Axial Force Variation

Before the experiment, monitoring the prestress of the anchor rods ensures their stable state, eliminating factors such as the relaxation of steel stress that could cause prestress loss [9]. The only controlled variable was rainfall.

Figure 6 shows the variation of anchor rod axial force at different depths over time. During the rainfall process, the axial force of anchor rods at different depths follows a consistent trend with rainfall duration. In the early stages of rainfall, the axial force of the anchor rods shows a linear increase. This is because rainwater infiltration increases the soil moisture content, significantly increasing the weight, and thereby increasing the sliding force of the slope. To resist slope movement, the axial force of the anchor rod increases. When rainfall has just stopped, due to the incomplete infiltration of some rainwater, the axial force of the anchor rod continues to increase for some time after rainfall cessation, but at a slower rate. In the mid-stage of rainfall, with continuous rainwater infiltration, the axial force of the anchor rod decreases significantly before stabilizing. This occurs because rainfall causes soil softening, which consequently diminishes shear strength and reduces the initial consolidation pressure of the upper soil layers. At the M2 location, the axial force decreases from 270 N to 150 N, showing a relatively large reduction during the infiltration phase. This indicates that rainwater infiltration has a significant impact on the axial force of the upper anchor rod. It is evident that rainfall has a substantial influence on the shallow soil of the loess slope reinforced with prestressed anchor rods, highlighting the need to strengthen the monitoring of the axial force of the upper anchor rod. In the later stages of rainfall, the axial force of the anchor rod fluctuates due to cracks accelerating water infiltration. The axial force shows a slight increase, and during the nighttime infiltration phase, the axial force slowly decreases again. Eventually, due to the collapse of the soil behind the retaining board and the loss of soil around the first-layer anchor rods, the reinforcement is exposed, leading to failure, and the axial force at M1 drops to 0 N.

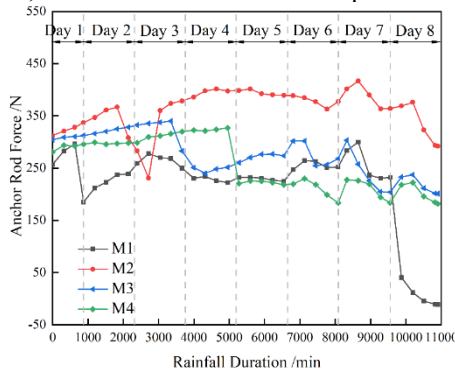


Fig. 6. Variation of Axial Force with Rainfall Duration

Figure 7 displays the variation of axial forces along the length of the third row of anchor rods at different time points. It is evident that the distribution pattern of axial forces along the length of the anchor rods during rainfall shows no significant changes.

The axial force in the free section of the anchor rod remains relatively constant along its length, while in the anchored section, the axial force follows a pattern of being larger in the middle and smaller at the ends. The maximum axial force is reached at a length of 0.85 m, and the axial force at the end of the anchor rod is 0 N. With the increase in rainfall duration, the overall axial force values at the same position gradually increase, followed by a decrease in the later stages of rainfall. This is attributed to the transition of the slope from unsaturated to locally saturated conditions from top to bottom as rainwater infiltrates during the early stages of rainfall. The matric suction in the unsaturated zone decreases and the effective stress increases, leading to vertical settlement and accompanying horizontal displacement. The support structure restricts the horizontal movement of the soil, causing an increase in axial force in the anchor rod. As rainwater infiltrates from top to bottom, the local saturation of the soil changes as follows: small  $\rightarrow$  large  $\rightarrow$  small. This results in a transition process of the soil experiencing local unsaturation  $\rightarrow$  local saturation  $\rightarrow$  local unsaturation. Rainwater infiltration also gradually reduces the frictional force between the anchor and the soil, causing a slight decrease in axial force. During the rainfall process, the effects on the axial forces at the end and middle of the anchored section are most significant. As the length of the anchor rod increases, the influence of rainfall on the axial forces gradually diminishes.

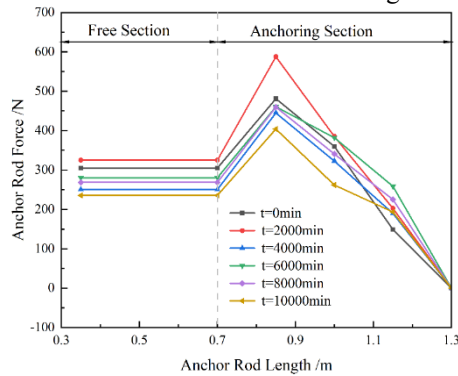


Fig. 7. Variation of Axial Force along the Length of the Anchor Rod

## 4 Failure Modes of Reinforced Loess Slopes with Frame Pre-stressed Anchors under Rainfall Influence

### 4.1 Evolution Characteristics of Slope Cracks

Cracks have a significant impact on loess slopes under rainfall conditions, not only compromising the overall integrity of the slope but also providing preferential pathways for rainwater infiltration, thereby accelerating the slope's failure process and adversely affecting the stability of loess slopes.

(1) With the infiltration of rainfall, small transverse cracks develop at the rear edge of the slope. This is a result of initial rainfall conditions, where rainwater infiltration increases the moisture content of the surface soil, reducing matric suction and leading

to the formation of a localized saturated zone. After rainfall ceases, the rainwater percolates downward, causing the particles in the surface soil to contract, increasing matric suction, and leading to shrinkage deformation of the surface soil. Intermittent rainfall keeps the surface soil in a state of alternating wetting and drying, causing uneven expansion and contraction. The deformation is limited by the tensile strength between soil particles, forming a tensile stress field on the surface of the soil. Local stress concentration occurs when the horizontal combined force exceeds the tensile strength between soil particles, resulting in the initiation of small cracks at the slope's top; this marks the initial incubation stage of cracks.

(2) As rainfall continues, the small cracks persist and expand, forming a thorough transverse tensile crack at the rear edge of the slope, directly above the end of the anchored section. This occurs because rainwater infiltration increases the moisture content, leading to soil softening and a decrease in shear strength. Additionally, the slope has an overhanging face. Under the combined action of the self-weight of the soil and percolation forces, the softened soil cannot sustain the existing load, resulting in a downward movement of the upper soil along the slope. The location of this crack indicates the anchoring effect of the prestressed anchor rod in the soil. Due to the restraint imposed by the retaining wall, with the increase in rainfall duration, the tensile crack does not continue to widen towards the overhanging face but allows rainwater to seep in, forming an erosive channel.

(3) Subsequently, longitudinal shear cracks develop at the rear midsection of the slope, continually extending towards the shoulder of the slope. The erosive channel on the right side also extends towards the midsection and shoulder. Due to the lower terrain at the eroded shoulder in the early stages, most of the accumulated water concentrates at the front edge of the slope. This makes the longitudinal crack at this stage the preferred infiltration pathway. Rainwater infiltration causes the crack to lengthen, widen, and deepen continuously. Since the displacement of the shear crack increases from the rear edge towards the front edge, in the absence of supporting structures, this landslide belongs to the type of traction landslide.

## 4.2 Failure Mode

Based on the analysis above, it is evident that the cracks at the rear edge of the slope are steep, and the slope top is relatively flat. When this slope lacks support structures, it would develop into a deep-seated landslide and fail. Later, due to the presence of support structures, it transforms into a top erosion, forming an erosive channel. The failure mode of the intermittent heavy rainfall-affected framed and anchored reinforced loess slope is illustrated in Figure 8, consisting of the following five stages:

(1) **Shoulder Erosion:** In the initial stages of rainfall, vertical settlement occurs in the front edge soil of the slope. Rainwater flows along the slope surface, concentrating at the front edge of the slope, leading to erosion of the slope shoulder. The erosion intensity gradually weakens from top to bottom, as shown in Figure 8(a).

(2) **Toe Erosion:** Rainwater flows into the gap between the retaining wall and the slope, and accumulates at the bottom of the slope without timely drainage, causing

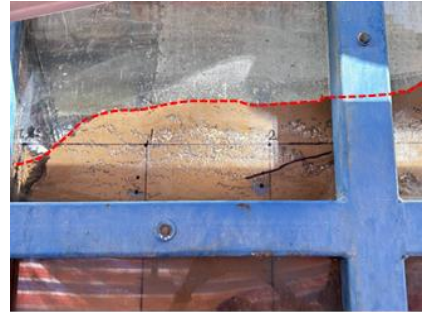
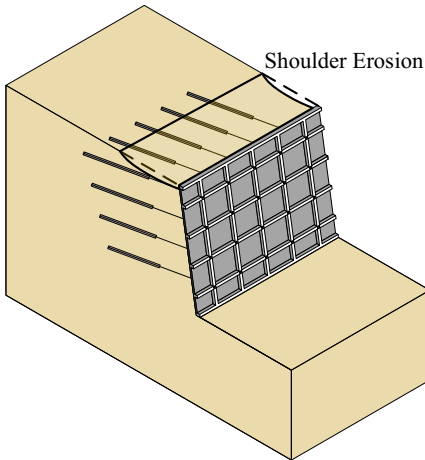
softening of the slope toe. This favors the formation of a weak surface at the slope toe, as shown in Figure 8(b).

(3) Formation and Development of Rear Edge Cracks: With the infiltration of rain-water, the moisture content increases, and the loess material softens, resulting in a reduction in shear strength. Under the influence of the self-weight of the soil and percolation forces, the softened soil cannot sustain the existing load, and the upper soil has a tendency to move downward along the slope surface. Eventually, transverse cracks form at the rear edge of the slope and gradually expand, as shown in Figure 8(c).

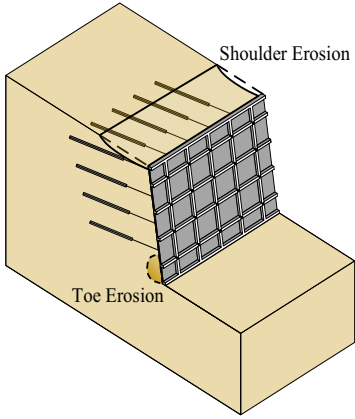
(4) Formation of Potential Slip Surface: Due to the extension of joints and the generation of cracks, the slope undergoes deformation. During the deformation process, some soil experiences poor drainage, resulting in excess pore water pressure and a reduction in effective stress. When the soil strength decreases to a critical value, a slip surface forms from the rear edge crack to the slope toe, as shown in Figure 8(d).

(5) Formation of Erosive Channel: Shear cracks gradually extend into the deeper and central parts of the slope, causing erosion and soil loss on the slope surface. An erosive channel forms in the middle of the slope shoulder, leading to the exposure of the first-layer anchor bars and subsequent failure, as shown in Figure 8(e).

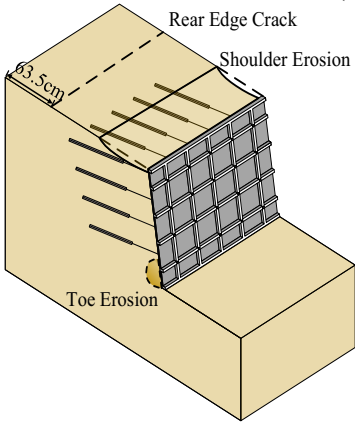
Through the comparative analysis with the experimental results of Zhang et al. [10], it is observed that the evolution characteristics of cracks in loess slopes under rainfall conditions are consistent before and after support. However, due to the restriction of the retaining wall, large-scale landslides did not occur, and the failure mode transformed from overall sliding to erosion-induced failure. Therefore, in practical engineering, it is essential to implement proper drainage measures at the slope top to avoid erosion-induced failure.



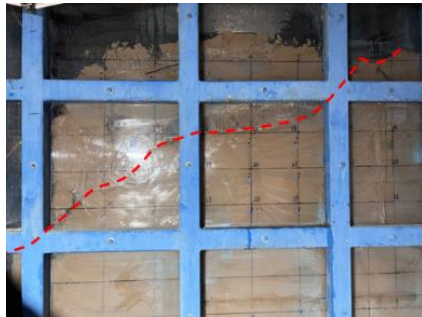
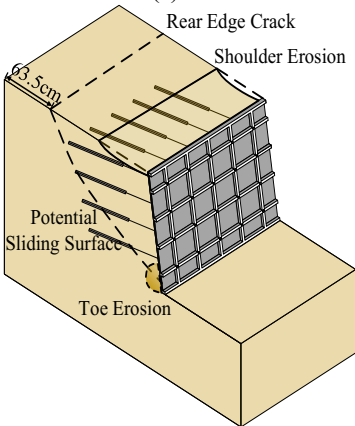
(a) Shoulder Erosion



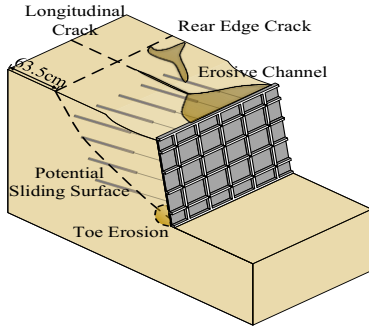
(b) Toe Erosion



(c) Formation and Development of Rear Edge Cracks



(d) Formation of Potential Slip Surface



(e) Formation of Erosive Channel

**Fig. 8.** Failure Mode of Framed and Anchored Reinforced Loess Slope under Intermittent Heavy Rainfall

## 5 Conclusion

In this study, the variations in slope volumetric water content, pore water pressure, anchor rod axial force are analyzed through the model test of framed prestressed anchor reinforced loess slope under rainfall, aiming to investigate its failure mode. The following conclusions are drawn:

(1) The change in volumetric water content of the slope is most directly impacted by rainfall. It exhibits a quasi-periodic variation during intermittent rainfall, rapidly increasing during rainfall, and decreasing during the infiltration phase. The overall trend of pore water pressure changes is generally consistent with volumetric water content, but the response of pore water pressure sensors to rainfall infiltration lags behind that of soil moisture sensors. With the increase of pore water pressure, the matrix suction decreases, which has a negative effect on the soil shear strength index. In practical engineering, the rainwater infiltration in slope can be reduced by increasing the compaction degree of the upper soil or opening drainage holes in the retaining plate.

(2) During simulated rainfall, the axial force of the anchor rod initially shows a linear increasing trend. As rainfall continues, the axial force decreases and eventually stabilizes. The distribution pattern of axial force along the length of the anchor rod does not undergo fundamental changes. The axial force in the free section remains essentially unchanged, while in the anchored section, it follows a pattern of being larger in the middle and smaller at both ends. In practical engineering, the bearing capacity of soil and the anchoring effect of the anchored section should be fully considered when designing the anchor rod.

(3) The instability process of the framed and anchored loess slope is manifested as follows: Rainfall infiltration → Significant weight and increased permeability of upper soil, reduced strength → Shoulder erosion → Toe softening and collapse → Transverse cracks at the rear edge of the slope top develop and progress → Formation of a potential sliding surface → Vertical shear cracks at the slope top develop and progress → Failure of the first row of steel bars caused by the loss of water and soil behind the retaining wall → Slope failure.

(4) The generation of cracks is critical to the formation of landslides. The evolution characteristics of cracks in loess slopes under rainfall conditions are consistent before and after reinforcement, but the failure mode significantly changes from overall sliding to erosion-induced failure. Therefore, attention should be paid to top drainage measures in practical engineering to reduce the occurrence of slope top cracks, providing references for the stability analysis and disaster prevention of loess slopes under rainfall conditions in loess regions.

## Acknowledgement

Fund Project: General Project of National Natural Science Foundation of China (51978321); Changjiang Scholars and Innovation Team Support Program of Ministry of Education (IRT\_17R51).

## References

1. Zhu Y P, Luo X H, Z Y. (2008) Support Structure Design. Higher Education Press. Beijing. <http://www.hep.com.cn>.
2. Sun Z L, Wen S J, Liang C, et al. (2020) A method for constructing and searching three-dimensional arbitrary slip surface based on minimum potential energy. *Rock and Soil Mechanics*, 41, S1:255-263. <https://doi.org/10.16285/j.rsm.2019.1252>.
3. Li N, Xu J C, Qin Y Z. (2012) Research on calculation model for stability evaluation of rainfall-induced shallow landslides. *Rock and Soil Mechanics*, 33, 05: 1485-1490. <https://doi.org/10.16285/j.rsm.2012.05.012>.
4. Kawai, K, Kijima, Y, Nakashima, K. (2020) Estimation of change in slope stability due to rainfall varied with time, based on unsaturated soil mechanics. *Geotechnics for Sustainable Infrastructure Development*, 62: 817-824. [https://doi.org/10.1007/978-981-15-2184-3\\_105](https://doi.org/10.1007/978-981-15-2184-3_105).
5. Di Matteo L, Pauselli C, Valigi D, et al. (2018) Reliability of water content estimation by profile probe and its effect on slope stability. *LANDSLIDES*, 15, 1: 173-180. <https://doi.org/10.1007/s10346-017-0895-7>.
6. Guo Z S, Zhao J B, Zhao Z Y. (2017) Stability Analysis of Slope Reinforced with Anti-slide Pile Under the Condition Rainfall Infiltration. *Journal of Civil Engineering and Management*, 34, 04: 47-52. <https://doi.org/10.13579/j.cnki.2095-0985.2017.04.008>.
7. Zou Y, Hu Z J, Mou H B, et al. (2017) Model test study on the effect of rainfall on long-term stability of loess slope with retaining wall. *Journal of Xi'an University of Science and Technology*, 42, 02: 299-306. <https://doi.org/10.13800/j.cnki.xakjdxxb.2022.0214>.
8. LIU G N, LI C, LU B, et al. (2020) Model Test on Shallow Failure of Fully and Strongly Weathered Rock Slope Induced by Rainfall. *Journal of Yangtze River Scientific Research Institute*, 37, 07: 88-95+104. <https://doi.org/10.11988/ckyyb.20190217>.
9. Zhou Y, Zhu Y P. (2010) Research on the anchor prestress loss of grillage flexible supporting structure with prestressed anchors. *Geotechnical Investigation & Surveying*, 38, 09: 1-6. <https://www.cnki.net/>.
10. Zhang S, Pei X J, Huang R Q, et al. (2019) Model test on seepage characteristics and deformation failure modes of loess fill slope under rainfall. *China Journal of Highway and Transport*, 32, 09: 32-41+50. <https://doi.org/10.19721/j.cnki.1001-7372.2019.09.003>.

**Open Access** This chapter is licensed under the terms of the Creative Commons Attribution-NonCommercial 4.0 International License (<http://creativecommons.org/licenses/by-nc/4.0/>), which permits any noncommercial use, sharing, adaptation, distribution and reproduction in any medium or format, as long as you give appropriate credit to the original author(s) and the source, provide a link to the Creative Commons license and indicate if changes were made.

The images or other third party material in this chapter are included in the chapter's Creative Commons license, unless indicated otherwise in a credit line to the material. If material is not included in the chapter's Creative Commons license and your intended use is not permitted by statutory regulation or exceeds the permitted use, you will need to obtain permission directly from the copyright holder.

